

Title	TiN/ZrO ₂ /Ti/Al metal-insulator-metal capacitors with subnanometer CET using ALD-deposited ZrO ₂ for DRAM applications
Authors	Monaghan, Scott;Cherkaoui, Karim;O'Connor, Éamon;Djara, Vladimir;Hurley, Paul K.;Oberbeck, L.;Tois, E.;Wilde, L.;Teichert, S.
Publication date	2009-02-10
Original Citation	Monaghan, S., Cherkaoui, K., O'Connor, É., Djara, V., Hurley, P. K., Oberbeck, L., Tois, E., Wilde, L. and Teichert, S, (2009) 'TiN/ZrO ₂ /Ti/Al metal-insulator-metal capacitors with subnanometer CET using ALD-deposited ZrO ₂ for DRAM applications', IEEE Electron Device Letters, 30(3), pp. 219-221. doi: 10.1109/LED.2008.2012356
Type of publication	Article (peer-reviewed)
Link to publisher's version	10.1109/LED.2008.2012356
Rights	© 2009, IEEE. Personal use of this material is permitted. Permission from IEEE must be obtained for all other uses, in any current or future media, including reprinting/republishing this material for advertising or promotional purposes, creating new collective works, for resale or redistribution to servers or lists, or reuse of any copyrighted component of this work in other works.
Download date	2024-05-05 04:10:24
Item downloaded from	https://hdl.handle.net/10468/13309



UCC

University College Cork, Ireland
Coláiste na hOllscoile Corcaigh

TiN/ZrO₂/Ti/Al Metal–Insulator–Metal Capacitors With Subnanometer CET Using ALD-Deposited ZrO₂ for DRAM Applications

S. Monaghan, K. Cherkaoui, É. O'Connor, V. Djara, P. K. Hurley, L. Oberbeck, E. Tois, L. Wilde, and S. Teichert

Abstract—We provide the first report of the structural and electrical properties of TiN/ZrO₂/Ti/Al metal–insulator–metal capacitor structures, where the ZrO₂ thin film (7–8 nm) is deposited by ALD using the new zirconium precursor ZrD-04, also known as Bis(methylcyclopentadienyl) methoxymethyl. Measured capacitance–voltage (C – V) and current–voltage (I – V) characteristics are reported for premetallization rapid thermal annealing (RTP) in N₂ for 60 s at 400 °C, 500 °C, or 600 °C. For the RTP at 400 °C, we find very low leakage current densities on the order of nanoamperes per square centimeter at a gate voltage of 1 V and low capacitance equivalent thickness values of ~ 0.9 nm at a gate voltage of 0 V. The dielectric constant of ZrO₂ is 31 ± 2 after RTP treatment at 400 °C.

Index Terms—ALD, capacitor, dynamic random access memory (DRAM), effective dielectric constant, gate oxide, high- k , metal–insulator–metal (MIM), ZrD-04, ZrO₂.

I. INTRODUCTION

THE METAL–INSULATOR–METAL (MIM) capacitor for dynamic random access memory (DRAM) and for other analog and radio-frequency applications is attracting great interest in recent times [1]–[3] and must be aggressively scaled to meet the expectations of the semiconductor roadmap [4]. This demands the replacement of SiO₂ with a high dielectric constant (k) oxide that will provide a capacitance equivalent thickness (CET¹) for the dielectric in the low subnanometer

regime and a leakage current density of less than 1 fA/cell, equivalent to approximately 1×10^{-8} – 1×10^{-7} A/cm².

Replacing SiO₂ ($k = 3.9$) with ZrO₂ ($k \sim 20$ – 40) is considered by the authors as an investigative step toward introducing favored Hf/Zr-based crystalline ternary oxides ($k > 40$) that will further reduce the CET value in line with current expectations [4]. Although DRAM MIM capacitor dielectrics with a CET of ~ 0.9 nm are currently being implemented by the semiconductor industry, the high- k values and the very low leakage current densities reported here presently allow a margin of opportunity for the ALD method to further reduce the physical thickness of the oxide and improve on the ~ 0.9 -nm CET while still maintaining acceptable leakage current densities [4].

II. SAMPLE DETAILS AND TECHNIQUE

The substrate is n-type silicon with n+ type As surface doping ($\sim 5 \times 10^{19}$ cm⁻³) of Si(100). This surface is exposed pre-MIM processing and forms a heavily As-doped SiO₂ layer, on which a layer of TiN metal (~ 10 nm) is formed by metal–organic chemical vapor deposition. An ~ 7 – 8 -nm thick ZrO₂ film is deposited by ALD in an ASM Pulsar 2000, hot wall cross-flow reactor, at a reaction temperature of 275 °C, using Bis(methylcyclopentadienyl) methoxymethyl zirconium (SAFC Hitech, ZrD-04, see [5]) and ozone as precursors. Crystallization to the preferred tetragonal ZrO₂ symmetry would maximize the dielectric constant and minimize the CET; hence, premetallization rapid thermal annealing (RTP) treatments are employed to investigate the optimum temperature for increasing the k -value without significantly increasing the leakage current density. RTP is carried out for 60 s in N₂ (1000-mbar) either at 400 °C, 500 °C, or 600 °C, using the Jipelec JetFirst 150 system. As-deposited samples (no RTP processing) are retained for comparative measurements. DRAM test MIM planar capacitors of various areas are formed from the as-deposited and RTP-treated samples using photolithography and a lift-off process for gate metallization. Device areas range from 400 to 160 000 μm^2 . The metal gate consists of 10 nm Ti and 200 nm Al, both deposited *ex situ* by e-beam. Ti, Al, and TiN are the preferred metals because they meet the basic industrial standards, such as acceptable work functions, good adhesion, low cost, good step coverage, high temperature stability, and low resistivity.

Capacitance voltage (C – V) and capacitor quality factor voltage (Q – V) measurements were performed at 25 °C using

Manuscript received June 26, 2008; revised December 23, 2008. This work was supported in part by the Sixth European Framework Programme under REALISE Project NMP4-CT-2006-016172, by the Science Foundation Ireland under Grant 05/IN/1751, by the Irish National Development Plan, and by the European Union Structural Funds. The review of this letter was arranged by Editor T. Wang.

S. Monaghan, K. Cherkaoui, É. O'Connor, V. Djara, and P. K. Hurley are with the Tyndall National Institute, University College Cork, Cork, Ireland (e-mail: scott.monaghan@tyndall.ie; karim.cherkaoui@tyndall.ie; eamon.oconnor@tyndall.ie; vladimir.djara@tyndall.ie; paul.hurley@tyndall.ie).

L. Oberbeck and S. Teichert are with Qimonda Dresden GmbH & Co. OHG, 01079 Dresden, Germany (e-mail: lars.oberbeck@qimonda.com; Steffen.Teichert@qimonda.com).

E. Tois is with the ASM Microchemistry Ltd., 00560 Helsinki, Finland (e-mail: eva.tois@asm.com).

L. Wilde is with the Fraunhofer Center for Nanoelectronic Technologies, 01099 Dresden, Germany (e-mail: WildeL.External@qimonda.com).

Digital Object Identifier 10.1109/LED.2008.2012356

¹The CET rule gives the same capacitance for a physically thicker high- k oxide layer, where $\text{CET} = 3.9\epsilon_0 A / C_{\text{high-}k}$. CET and the equivalent oxide thickness ($\text{EOT} = 3.9t_{\text{high-}k} / k_{\text{high-}k}$) are approximately equal for MIM devices; hence, we can use this to get an effective value for $k_{\text{high-}k} (k_{\text{eff}})$. Hence, $k = k_{\text{high-}k} \sim k_{\text{eff}}$.

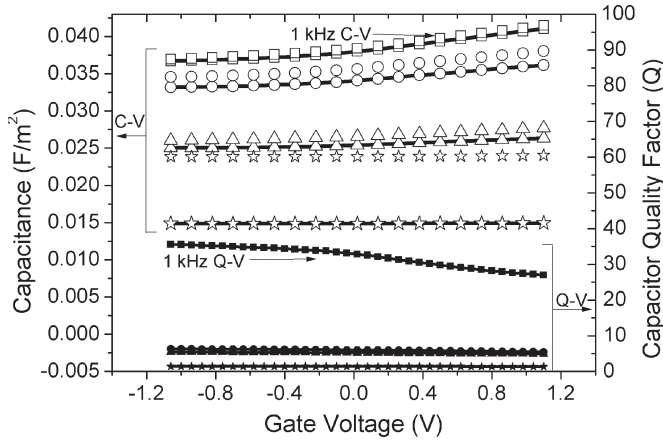


Fig. 1. (Open symbols) C - V and (filled symbols) related Q - V responses for a low leakage current density device of area $40\,000\,\mu\text{m}^2$ with RTP at $400\,^\circ\text{C}$. (Squares) One kilohertz. (Circles) Ten kilohertz. (Triangles) One hundred kilohertz. (Stars) One megahertz. Symbols connected with lines represent the parallel capacitance responses, and symbols with no lines are the series capacitance responses. The 1 kHz responses are almost superimposed, whereas C_p and C_s at other frequencies are dispersed due to the effects of series resistance. The slight bow in the 1 and 10 kHz C - V 's is due to nonsymmetric metal work functions and dependences of the quadratic voltage coefficient of the capacitance (α) [1]–[3].

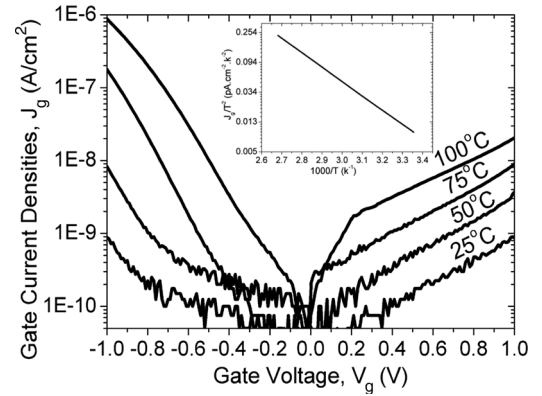


Fig. 2. Gate leakage current (J - V) plots for $40\,000\,\mu\text{m}^2$ area devices with an RTP of $400\,^\circ\text{C}$. Measurement temperatures (T_m) are $25\,^\circ\text{C}$, $50\,^\circ\text{C}$, $75\,^\circ\text{C}$, and $100\,^\circ\text{C}$. At $25\,^\circ\text{C}$, J is approximately $1 \times 10^{-9}\,\text{A}/\text{cm}^2$ at 1 V. The dominant conduction mechanism for all positive gate voltages up to 1 V is SE, and the dominant conduction mechanisms for negative gate voltages at $T_m = 25\,^\circ\text{C}$ are PF emissions in the range of -0.8 to -1 V, and SE in the range of 0 to -0.8 V. It can be seen that PF becomes increasingly dominant over SE in the range of 0 to -0.8 V as T_m increases, consistent with the lower work function of Ti compared with TiN. (Inset) SE's linear relationship of J/T^2 versus $10^3/T$ ($V_g = 1$ V), with an activation energy of ~ 0.4 eV and a TiN/ZrO₂ barrier height of ~ 1.4 eV.

73 an HP4284A Precision LCR Meter. Current–voltage (I - V)
74 measurements were performed with an HP4156A Precision
75 Semiconductor Parameter Analyzer. I - V measurements were
76 recorded at $25\,^\circ\text{C}$, $50\,^\circ\text{C}$, $75\,^\circ\text{C}$, and $100\,^\circ\text{C}$. All measurements
77 were performed on-wafer in a microchamber probe station
78 (Cascade Microtech, model Summit 12971B) in a dry-air en-
79 vironment (dew point $\sim -70\,^\circ\text{C}$).

III. MEASUREMENTS AND RESULTS

81 Before using results from multifrequency C - V responses,
82 it is necessary to establish the effects of series resistance at
83 different frequencies. An established method is to compare the
84 series capacitance–voltage (C_s - V) response with the parallel
85 capacitance–voltage (C_p - V) response. If the C - V responses
86 differ in low leakage current density devices, then this is due to
87 series resistance effects.

88 Fig. 1 shows the C - V and Q - V responses for a low leakage
89 device of area $160\,000\,\mu\text{m}^2$ having undergone an RTP of
90 $400\,^\circ\text{C}$. The 1 kHz responses are almost identical, whereas
91 the 10, 100, and 1 MHz responses are affected by series
92 resistance. In addition, Q values are good for the 1 kHz
93 responses (~ 30) but reduce rapidly as the frequency is in-
94 creased. Transmission electron microscopy (TEM) energy dis-
95 persive X-ray spectroscopy shows a 10–20 nm SiO₂ layer
96 between the Si substrate and the TiN layer, which has a
97 high As doping. The thickness of this interlayer does not
98 increase with RTP treatment; however, its presence gives a
99 substrate resistivity/higher resistivity film underneath the TiN
100 layer and is the likely cause of the series resistance ef-
101 fects for frequencies > 1 kHz. Hence, information extracted
102 from C - V responses is confined to the 1 kHz measure-
103 ments, which are sufficient for electrical characterization.
104 Other higher frequency C - V data are ignored. The ob-
105 served C - V frequency dispersion for frequencies greater than

1 kHz is more pronounced for devices with larger areas 106
($\sim 0.005\,\text{F}/\text{m}^2$ range $\rightarrow \sim 0.03\,\text{F}/\text{m}^2$ range) and is also more 107
pronounced for devices processed with higher RTP tempera- 108
tures ($\sim 0.013\,\text{F}/\text{m}^2$ range $\rightarrow \sim 0.025\,\text{F}/\text{m}^2$ range). In addition, 109
the Q - V responses show reductions in Q by at least an order 110
of magnitude for devices with larger areas and for devices 111
processed with higher RTP temperatures. It is noted, however, 112
that leakage current densities for all devices remain low on the 113
order of nanoamperes per square centimeter and scale with the 114
device area; hence, the leakage current is not a contributing 115
factor to the observed frequency dispersion. 116

Leakage current densities (J - V) at 1 V for all devices 117
(except RTP at $600\,^\circ\text{C}$) are low at ~ 1 – $2 \times 10^{-9}\,\text{A}/\text{cm}^2$ for a 118
measurement temperature (T_m) of $25\,^\circ\text{C}$. This would indicate 119
that C contamination is low [6]. The J - V of devices with an 120
RTP of $600\,^\circ\text{C}$ increases to $\sim 3 \times 10^{-8}\,\text{A}/\text{cm}^2$ ($T_m = 25\,^\circ\text{C}$) for 121
all device areas. Fig. 2 shows J - V plots for a $40\,000\,\mu\text{m}^2$ area 122
device with an RTP of $400\,^\circ\text{C}$. The conduction mechanisms at 123
 $V_g = 1$ V and -1 V are Schottky (SE) and Poole–Frenkel (PF) 124
emissions, respectively (see Fig. 2 inset for SE details). 125

Fig. 3 shows X-ray diffraction (XRD) data for as-deposited 126
and RTP-treated devices. The inset also shows a TEM mi- 127
crograph of a post-RTP of $600\,^\circ\text{C}$ device. Considering these 128
data with the k values shown in Fig. 4, there seems to be 129
cubic/tetragonal crystallites contained within an amorphous 130
structure. As the RTP temperature increases, the k value in- 131
creases, possibly due to a cubic-to-tetragonal phase change 132
due to contaminants, such as F becoming less influential on 133
the crystalline phase [6]. The high leakage at the $600\,^\circ\text{C}$ 134
RTP is likely due to the higher k polycrystalline structure 135
forming grain boundaries [7] and, possibly, Ti diffusion into 136
the oxide via the TiO interlayer formation at the TiN/ZrO₂ 137
interface [8]. Interlayer roughness can also increase with the 138
RTP temperature, as seen from TEM, where ZrO₂ will follow 139
the crystallization grains of TiN and Ti metals. However, this 140

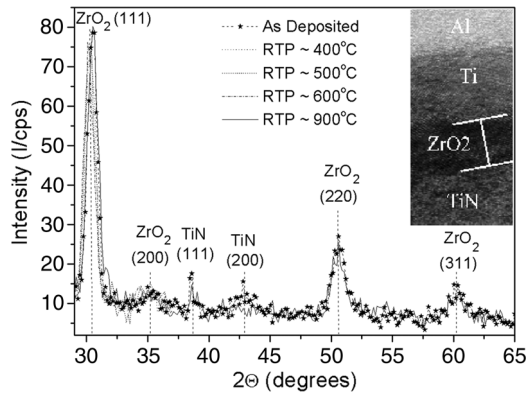


Fig. 3. XRD data conducted at room temperature for the as-deposited and post 900 °C RTP devices ($2\theta = 29^\circ - 65^\circ$) and at $\sim 400^\circ\text{C}$, $\sim 500^\circ\text{C}$, and $\sim 600^\circ\text{C}$ *in situ* for the equivalent RTP devices ($2\theta = 25^\circ - 37^\circ$). The dominant response at $\sim 30^\circ$ shows a significant cubic and/or tetragonal crystalline contribution which does not change significantly with RTP processing. (Inset) TEM micrograph of a post-RTP of 600 °C device.

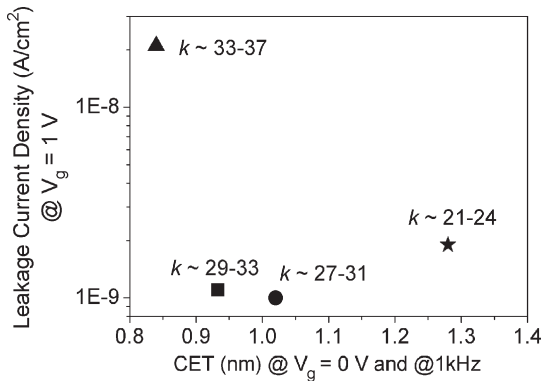


Fig. 4. CET values extracted from 1 kHz $C-V$ responses at $V_g = 0\text{ V}$, plotted against leakage current densities at $V_g = 1\text{ V}$. The calculated dielectric constants are also shown. (Star) As-deposited devices. (Square) Four-hundred-degree-Celsius RTP devices. (Circle) Five-hundred-degree-Celsius RTP devices. (Triangle) Six-hundred-degree-Celsius RTP devices. The physical thickness of ZrO₂ remains unchanged for all devices at 7–8 nm.

does not affect the device performance at or below an RTP of 500 °C [7].

Fig. 4 shows CET values extracted from 1 kHz $C-V$ responses at $V_g = 0\text{ V}$, plotted against leakage current densities at $V_g = 1\text{ V}$. The estimated k -value ranges for ZrO₂ are included, indicating an increase in k with RTP processing ($22.5 \pm 1.5 \rightarrow 32 \pm 5$) and an associated reduction in CET with RTP processing ($\sim 0.3\text{ nm}$). However, the leakage current density increases ($> 1 \times 10^1$) following the 600 °C RTP processing. These results compare well with a recent study [6], apart from the lower

leakage observed here for all devices except those with the 600 °C RTP processing.

IV. CONCLUSION

MIM capacitors (TiN/ZrO₂/Ti/Al), having the oxide formed by ALD with the new ZrD-04 precursor, are investigated for the first time. $C-V$ frequency dispersion ($> 1\text{ kHz}$) is observed, which is more pronounced for devices with larger areas and with higher RTP temperatures. $Q-V$ responses reduce by at least an order of magnitude with increasing frequency. The leakage current densities at 1 V for all devices (except 600 °C RTP) are on the order of nanoamperes per square centimeter. Devices with an RTP of 600 °C show an unacceptable increase in the leakage current density by at least an order of magnitude. CET and k values are extracted using the 1 kHz $C-V$ responses and TEM micrographs. There is an increase in k with RTP processing ($22.5 \pm 1.5 \rightarrow 32 \pm 5$), with an associated reduction in CET with RTP processing ($\sim 0.3\text{ nm}$) toward the subnanometer regime. The best CET-leakage values for post-RTP (400 °C–500 °C) are $\sim 0.9\text{ nm}$ and $\sim 1 \times 10^{-9}\text{ A/cm}^2$, respectively. As the leakage current density values obtained at 1 V are below the target of $1 \times 10^{-8} - 1 \times 10^{-7}\text{ A/cm}^2$, there remains scope for further reduction in CET with ZrO₂ MIM structures formed by ALD with the new ZrD-04 precursor.

REFERENCES

- [1] C. Zhu, H. Hu, X. Yu, S. J. Kim, A. Chin, M.-F. Li, B. J. Cho, and D. L. Kwong, "Voltage and temperature dependence of capacitance of high- k HfO₂ MIM capacitors: A unified understanding and prediction," in *IEDM Tech. Dig.*, 2003, pp. 879–882.
- [2] S. J. Kim, B. J. Cho, M.-F. Li, S.-J. Ding, M. B. Yu, B. Narayanan, A. Chin, and D.-L. Kwong, "Improvement of voltage linearity in high- k MIM capacitors using HfO₂–SiO₂ stacked dielectric," *IEEE Electron Device Lett.*, vol. 25, no. 8, pp. 538–540, Aug. 2006.
- [3] F. El Kamel, P. Gonon, and C. Vallée, "Experimental evidence for the role of electrodes and oxygen vacancies in voltage nonlinearities observed in high- k MIM capacitors," *Appl. Phys. Lett.*, vol. 91, no. 17, p. 172 909, Oct. 2007.
- [4] "The international technology roadmap for semiconductors," *Process Integration, Devices, and Structures*, pp. 29–35, 2007.
- [5] J. W. Elam, M. J. Pellin, S. D. Elliott, A. Zydor, M. C. Faia, and J. T. Hupp, "Mechanism for zirconium oxide atomic layer deposition using Bis(methylcyclopentadienyl) methoxymethyl zirconium," *Appl. Phys. Lett.*, vol. 91, no. 25, p. 253 123, Dec. 2007.
- [6] J.-H. Kim, V. Ignatovaa, P. Küchera, J. Heitmannb, L. Oberbeck, and U. Schröder, "Physical and electrical characterization of high- k ZrO₂ metal-insulator-metal capacitor," *Thin Solid Films*, vol. 516, no. 23, pp. 8333–8336, Oct. 2008.
- [7] S.-W. Jeong, H. J. Lee, K. S. Kim, M. T. You, Y. Roh, T. Noguchi, W. Xianyu, and J. Jung, "Effects of annealing temperature on the characteristics of ALD-deposited HfO₂ in MIM capacitors," *Thin Solid Films*, vol. 515, no. 2, pp. 526–530, Oct. 2006.
- [8] L. Oberbeck, private communication.